



## Efficient and selective removal of cesium from aqueous solution using copper hexacyanoferrate nanoparticles supported on poly(methacrylic acid-co-itaconic acid)

Salah M. El-Bahy<sup>a,\*</sup>, Mohammed T. Alotaibi<sup>a</sup>, Amal M. Metwally<sup>b,\*</sup>

<sup>a</sup>Department of Chemistry, Turabah University College, Taif University, P.O. Box: 11099, Taif 21944, Saudi Arabia, emails: s.elbahy@tu.edu.sa (S.M. El-Bahy), Mtotaibi@tu.edu.sa (M.T. Alotaibi)

<sup>b</sup>Chemistry Department, Faculty of Science, Benha University, Benha, Egypt, email: anl.metwaly@fsc.bu.edu.eg

Received 14 February 2021; Accepted 7 July 2021

### ABSTRACT

A new poly(methacrylic acid-co-itaconic acid) [poly(MAA-co-IA)] hydrogel encapsulated copper hexacyanoferrate (CuHCF) nanoparticles was synthesized. The prepared samples were characterized by Fourier-transform infrared spectroscopy, scanning electron microscopy, energy-dispersive X-ray, transmission electron microscopy, X-ray diffraction, and thermogravimetric analysis–differential scanning calorimetry. The prepared composite CuHCF/poly(MAA-co-IA) was examined for adsorption of Cs<sup>+</sup> by batch technique. The effect of various factors like solution pH, Cs<sup>+</sup> initial concentration, agitation time, the temperature of the solution, and competition ions was investigated. CuHCF/poly(MAA-co-IA) composite exhibited high adsorption capacity (1.48 mmol g<sup>-1</sup>) of Cs<sup>+</sup> occur at a pH equal to 9, initial concentration of 8 mmol L<sup>-1</sup> Cs<sup>+</sup> at room temperature (25°C). The adsorption of Cs<sup>+</sup> was kinetically rapid, and the equilibrium was reached within 40 min. Between Langmuir, Freundlich, Temkin, and Dubinin–Radushkevich isotherms models, the data were well fitted with the Langmuir model, suggesting that the uptake of Cs<sup>+</sup> was monolayer and homogeneous. The adsorption kinetics parameters were fitted well to the pseudo-second-order model, and the Elovich equation indicated that chemisorption is the predominant adsorption mechanism. The intraparticle diffusion model shows that more than one controlling step may influence Cs<sup>+</sup> loading. Thermodynamic parameters were calculated in the temperature range of 25°C–55°C and revealed that Cs<sup>+</sup> sorption was endothermic, spontaneous, and more favourable at the higher temperature. The selectivity of the composite for Cs<sup>+</sup> in the existence of Na<sup>+</sup> and K<sup>+</sup>, Li<sup>+</sup>, Ca<sup>++</sup> Mg<sup>++</sup> ions was exceptional. Up to 98% desorption of Cs<sup>+</sup> was completed with 2M KCl.

*Keywords:* Itaconic acid; Methacrylic acid; Selective; Adsorption; Cs<sup>+</sup>; Batch method; Desorption

### 1. Introduction

Nuclear energy is a reliable and carbon-free energy source impacting the alleviation of global warming. But past nuclear disasters and radioactive incidents have reminded us of the amount of radioactive waste [1]. Representatively, in 2011, the nuclear disaster occurs at the Fukushima Daiichi

nuclear power station in Japan, which caused that radionuclides to contaminate the biosphere and spreads over a large area, including soil and seawater [1,2]. <sup>137</sup>Cs is considered one of the most abundant radionuclides produced from the fission process of uranium with a strong gamma emitter. It is one of the major hazardous radioactive because of the long half-life, which reached 30.2 y [3,4]. Also, the <sup>137</sup>Cs in

\* Corresponding authors.

aqueous solutions are chemically like potassium due to high solubility in water, so they spread through the environment and remains for a long time [5–7]. Cs<sup>+</sup> exist in very low concentration, below 0.1% and in large volume of radioactive Cs<sup>+</sup> contaminated wastewater compared to other competitive ions like Na<sup>+</sup>, K<sup>+</sup>, Mg<sup>2+</sup>, and Ca<sup>2+</sup> [8,9]. Consequently, it is challenging to selectively uptake of Cs<sup>+</sup> from the natural environment. There are many techniques to remove these radionuclides, containing ion exchange, precipitation, adsorption, solvent extraction, evaporation/concentration, chromatography, and electrochemical, that have been developed [9–13]. Ion exchange and adsorption are considered the greatest effective methods for the selective removal of Cs<sup>+</sup> due to their practical advantages, such as effective, facile, and high capacitive properties [14–16]. Various adsorbents such as aluminium molybdophosphate [17], calixarene [18], zeolites [19], silicotitanates [20] have been formerly examined for removal of Cs<sup>+</sup>, but these adsorbents are expensive or have low selectivity. Hexacyanoferrates (HCF) containing transition metals such as copper [14–16,21,22], nickel [23–25], iron [26,27], zinc [28], and cobalt [13] have been used for the uptake of Cs<sup>+</sup> ions from aqueous media because of its simple preparation, low cost, and high adsorption performance for Cs<sup>+</sup> ions. Due to the crystal structure of metal hexacyanoferrates (MHCF) with a channel diameter of around 3.2 Å, it accelerates the permeate of a smaller hydrated radius like Cs<sup>+</sup>. In contrast, the larger hydrated ions such as Mg<sup>+</sup> and Ca<sup>2+</sup> cannot exchange [22–26]. The uptake of Cs<sup>+</sup> in MHCF occurs by ion exchange with K<sup>+</sup>, present in the MHCF crystal [21–24]. The small particle size of MHCF may cause a significant drawback, mainly due to the required filtration step, and due to the complications of using this adsorbent in the column method. To overcome this disadvantage various approaches have been developed such as grafting MHCF to porous materials by encapsulation in polymer matrices [14,23,27–29]. The formation of the composite was able to overcome this disadvantage of nanoparticle adsorbents. Encapsulation of MHCF into a polymer matrix was done using various polymers such as poly(vinyl alcohol) [14], cellulose [23], chitin [26], polyacrylonitrile [27], and carbomer [29]. In our previous work, carbomer encapsulated potassium copper hexacyanoferrate (CuHCF) composite was prepared for removal of Cs<sup>+</sup> with high adsorption capacity (1.74 mmol g<sup>-1</sup>) and fast adsorption time (60 min) [29].

In this work, CuHCF/poly(methacrylic acid-co-itaconic acid) [poly(MAA-co-IA)] composite was synthesized with a low-cost and effective method. The characterization by Fourier-transform infrared spectroscopy (FTIR), scanning electron microscopy (SEM), energy-dispersive X-ray (EDX), X-ray diffraction (XRD), and thermogravimetric analysis–differential scanning calorimetry (TGA–DSC) was investigated for studying the composite composition, properties, and morphology. The adsorption of Cs<sup>+</sup> onto CuHCF/poly(MAA-co-IA) composite was studied by batch technique. The amount of Cs<sup>+</sup> adsorbed was examined as a function of different factors like pH, Cs<sup>+</sup> concentration, contact time, the temperature of Cs<sup>+</sup> solution, and competition ions. Various adsorption isotherm models and kinetic models were examined. The effect of different eluents in the elution of adsorbed Cs<sup>+</sup> ions from the adsorbent was studied.

## 2. Materials and methods

### 2.1. Materials

Itaconic acid (IA), methacrylic acid (MAA), N,N'-methylenebis(acrylamide) (NMBA), and polyvinyl alcohol (PVA) were purchased from Sigma-Aldrich (USA). Potassium persulphate (K<sub>2</sub>S<sub>2</sub>O<sub>8</sub>), lithium chloride (LiCl), sodium chloride (NaCl), calcium chloride (CaCl<sub>2</sub>), magnesium chloride (MgCl<sub>2</sub>) was obtained from Merck, (India). CsCl was obtained from Alfa Aesar (USA) (CuSO<sub>4</sub>·5H<sub>2</sub>O), (K<sub>4</sub>[Fe(CN)<sub>6</sub>]<sub>3</sub>·3H<sub>2</sub>O) were bought from Sigma-Aldrich (USA).

### 2.2. Synthesis of CuHCF/poly(MAA-co-IA) composite

#### 2.2.1. Synthesis of nanoparticles of CuHCF

CuHCF powder was synthesized by the reaction of a solution of copper sulfate (10 wt.%) with a solution of potassium hexacyanoferrate (KHCF) (10 wt.%) in the existence of PVA as a stabilizer (6 wt.%) in an aqueous solution. The copper sulfate solution was poured dropwise into the KHCF solution with constant stirring. The brown-coloured precipitate of CuHCF started to appear on the mixing of the two solutions. The fine particles of CuHCF were separated by ultracentrifugation and washed with water several times. This residue was air-dried to obtain fine particles of CuHCF.

#### 2.2.2. Preparation of poly(MAA-co-IA)

Poly(MAA-co-IA) hydrogel was prepared by mixing 2 g of MAA and 0.5 g of IA in an aqueous media, including 0.025 g of NMBA (crosslinking agent) and 0.005 g of potassium persulphate (K<sub>2</sub>S<sub>2</sub>O<sub>8</sub>) as initiator. It was then bubbling mixture with nitrogen gas for 50 min to remove dissolved oxygen. Polymerization was performed at 60°C for 4 h. I was washing hydrogel with deionized water to remove unreacted monomers. Subsequently, hydrogel samples were dehydrated in an oven at 50°C for 24 h under vacuum to obtain the poly(MAA-co-IA) hydrogel.

#### 2.2.3. Synthesis of CuHCF/poly(MAA-co-IA) composite

Solution X was formed by dispersion of (2 g) of colourless powder of poly(MAA-co-IA) hydrogel in 50 mL of distilled water. Solution Y was formed by dispersing (3 g) of CuHCF in 50 mL distilled water. The two Solutions X and Y were mixed and shaken for 24 h. Ultracentrifugation, then washed with water several times to obtain the composite. The prepared composite was allowed to dry at 50°C for 24 h under vacuum, and it was mentioned as CuHCF/poly(MAA-co-IA) composite.

### 2.3. Characterization techniques

The FTIR spectra of the synthesized poly(MAA-co-IA) hydrogel, nanoparticles CuHCF and CuHCF/poly(MAA-co-IA) composite were measured using FTIR-BRUKER, Vector 22 (Germany) Spectrophotometer in KBr phase in the spectral range of 4,000–400 cm<sup>-1</sup>. Morphology of the synthesized samples was investigated using a field-emission

scanning electron microscope attached with EDX (ZEISS Sigma 300 VP, Germany) at an acceleration voltage of 10 kV. Also, the morphology and particle size of CuHCF were determined using transmission electron microscopy (TEM) (JEOL, JEM-1230 electron microscopy, Japan), the sample was prepared by the dispersion of fine particles in water under ultra-sonication and then one drop of the suspension was taken and evaporated on a carbon-coated copper grid and placed in the Phillips (CM/TEM). The thermal behaviors of the prepared poly(MAA-co-IA) hydrogel and CuHCF/poly(MAA-co-IA) composite were studied using SDT Q600 V20.5 Build 15 thermogravimetric analyzer in a dynamic atmosphere of nitrogen from room temperature to 1,000°C at a heating rate of 10°C/min. The X-ray diffraction of poly(MAA-co-IA) hydrogel and CuHCF/poly(MAA-co-IA) composite were studied by Diano X-ray diffractometer (USA) using Cu K $\alpha$  radiation ( $\lambda = 1.5418 \text{ \AA}$ ).

#### 2.4. Cs<sup>+</sup> removal by batch method

The sorption of nonradioactive Cs<sup>+</sup> (<sup>133</sup>Cs) using the new composite was investigated by batch technique, 0.1 g of CuHCF/poly(MAA-co-IA) composite was equilibrated with 100 mL of the prepared Cs<sup>+</sup> solution (CsCl) of known concentration (initial concentration) in polypropylene bottle. The mixture was shaken using a thermostat rotary shaker with a shaking speed of 250 rpm for 120 min at 25°C unless otherwise stated. The Cs<sup>+</sup> loaded composite was separated by filtration. After equilibration, the final amount of Cs<sup>+</sup> in the aqueous media was measured using an inductively coupled plasma optical emission spectrometry (ICP-OES) spectrometer. Each experiment was repeated three times to verify the precision of the obtained data. The influence of pH on Cs<sup>+</sup> uptake was studied by mixing 100 mL of Cs<sup>+</sup> solution (3 mmol L<sup>-1</sup>) with 0.1 g of a composite at different pH values ranging from 2 to 12. Solutions of 0.1 M HNO<sub>3</sub> and 0.1 M NaOH were used to adjust the desired pH of Cs<sup>+</sup> solutions. The influence of concentration on Cs<sup>+</sup> adsorption was investigated at a different initial concentration of Cs<sup>+</sup> in the range of 1–10 mmol L<sup>-1</sup> and optimum pH. The effect of shaking time on adsorption of Cs<sup>+</sup> was studied at different times (10–60 min), optimum pH, and optimum concentration of Cs<sup>+</sup>. The influence of temperature on the Cs<sup>+</sup> uptake was performed at temperatures 25°C, 35°C, 45°C, and 55°C, at optimum pH and 1.0 mmol L<sup>-1</sup> of Cs<sup>+</sup>. The effect of competing ions such as K<sup>+</sup>, Cs<sup>+</sup>, Li<sup>+</sup>, Na<sup>+</sup>, Ca<sup>2+</sup> and Mg<sup>2+</sup> (as mixed chloride solutions) on Cs<sup>+</sup> adsorption onto CuHCF/poly(MAA-co-IA) was studied. The experiment was performed by shaking 0.1 g of composite with 100 mL of the solution containing (1.0 mmol L<sup>-1</sup>) of each metal ion at optimum pH.

#### 2.5. Elution of Cs<sup>+</sup>

Adsorption of Cs<sup>+</sup> onto CuHCF/poly(MAA-co-IA) was occur by shaking 0.1 g of composite with 100 mL (3 mmol L<sup>-1</sup>) of Cs<sup>+</sup> solution for 60 min. After saturation of the composite with Cs<sup>+</sup>, the composite was filtered and air-dried at room temperature. The amount of Cs<sup>+</sup> adsorbed at equilibrium was calculated as previously mentioned. Desorption of sorbed Cs<sup>+</sup> was examined using H<sub>2</sub>O, NaCl, NaOH, KOH, KCl, and

HNO<sub>3</sub> (1 and 2 M) solutions. Desorption was performed by shaking the Cs<sup>+</sup>-saturated composite with 100 mL of the desorbing reagent in a shaker for 60 min at a shaking speed of 250 rpm. The Cs<sup>+</sup> concentration in the desorbed solutions was analyzed with an ICP-OES spectrometer.

#### 2.6. Theory/calculation

##### 2.6.1. Adsorption capacity

The adsorption capacity of Cs<sup>+</sup> onto composite,  $q_e$  (mmol g<sup>-1</sup>) was calculated using the following equation [29].

$$q = \frac{(C_o - C_e)V}{W} \quad (1)$$

where  $C_o$  (mmol L<sup>-1</sup>) and  $C_e$  (mmol L<sup>-1</sup>) are concentration before and after adsorption, respectively;  $V$  (L) is the volume of solution containing Cs<sup>+</sup>, and  $W$  is the weight of composite (g).

##### 2.6.2. Adsorption isotherm models

The mechanism of the adsorption process can be explained by applying isotherm models. Four isotherm models, namely, Langmuir [Eq. (2)] [30], Freundlich [Eq. (3)] [31], Temkin [Eq. (4)] [32], and Dubinin–Radushkevich (D–R) [Eq. (5)] [33], can be used to investigate the diffusion of the ions between the aqueous media and the adsorbent. Some information is given after applying the models, such as the affinity of the ions, properties of the adsorbent surface, uptake of metal ions, and mechanism of the adsorption process.

$$\frac{C_e}{q} = \frac{C_e}{Q_{\max}} + \frac{1}{K Q_{\max}} \quad (2)$$

$$\log q = N \log C_e + \log K_F \quad (3)$$

$$q = B \ln K_T + B \ln C_e \quad (4)$$

$$\ln q_e = \ln Q_{\max} - K_{DR} \varepsilon^2 \quad (5)$$

where  $C_e$  (mmol L<sup>-1</sup>) is the amount of metal ions after adsorption;  $q$  and  $Q_{\max}$  (mmol g<sup>-1</sup>) are the adsorption capacity at equilibrium and maximum adsorption capacity, respectively.  $K$  (L mmol<sup>-1</sup>) is the Langmuir constant;  $K_F$  (mmol g<sup>-1</sup>) and  $N$  are the Freundlich constants.  $K_T$  (L g<sup>-1</sup>) is constant related to equilibrium binding, and  $B$  (J mol<sup>-1</sup>) is constantly associated with the heat of adsorption.  $K_{DR}$  (mol<sup>2</sup> kJ<sup>-2</sup>) is a constant which is associated with the mean free energy of adsorption,  $\varepsilon$  (J mol<sup>-1</sup>) denotes the Polanyi potential, which is associated with concentration at equilibrium ( $C_e$ ) as indicated in the following equation:

$$\varepsilon = RT \ln \left( 1 + \frac{1}{C_e} \right) \quad (6)$$

Langmuir's model was studied to verify homogeneous adsorption. The essential characteristics of the Langmuir

model were expressed in terms of dimensionless constant ( $R_L$ ), which is calculated to expect the attraction between the ions and composite. The  $R_L$  value was estimated as follows:

$$R_L = \frac{1}{1 + KC_o} \quad (7)$$

The shape of the isotherm was predicted by  $R_L$  values. Since the isotherm is favorable when  $0 < R_L < 1$ , unfavorable when  $R_L > 1$ , linear when  $R_L = 1$ , and irreversible when  $R_L = 0$  [34].

To illustrate heterogeneous adsorption, the Freundlich adsorption model was used. The third isotherm model is the Temkin model, which assumes that the heat of adsorption of ions decreases linearly with coverage caused by indirect adsorbate–adsorbate interactions. The fourth isotherm model is the D–R model used to express the adsorption mechanism with a Gaussian energy distribution onto a heterogeneous surface.

### 2.6.3. Adsorption kinetic models

The kinetic process of adsorption of  $\text{Cs}^+$  by CuHCF/poly(MAA-co-IA) can be investigated by using four kinetic models: pseudo-first-order [Eq. (8)] [35], pseudo-second-order [Eq. (9)] [36], intraparticle diffusion model [Eq. (10)] [37], and Elovich equation [Eq. (11)] [38].

$$\log(q - q_t) = \log q - \left( \frac{K_{\text{ads}}}{2.303} \right) t \quad (8)$$

$$\frac{t}{q_t} = \frac{1}{K_2 q^2} + \left( \frac{1}{q} \right) t \quad (9-1)$$

$$h = K_2 q^2 \quad (9-2)$$

$$q_t = K_{\text{id}} t^{0.5} + C \quad (10)$$

$$q_t = \frac{1}{\beta} \ln(\alpha\beta) + \frac{1}{\beta} \ln t \quad (11)$$

where  $q$  and  $q_t$  are capacities of  $\text{Cs}^+$  adsorbed per gram of adsorbent ( $\text{mmol g}^{-1}$ ) at equilibrium and at any time  $t$  (min), respectively;  $K_{\text{ads}}$  ( $\text{min}^{-1}$ ),  $K_2$  ( $\text{g mmol}^{-1} \text{min}^{-1}$ ) and  $K_{\text{id}}$  ( $\text{mmol g}^{-1} \text{min}^{-0.5}$ ) are the rate constants of the first-order, second-order and intraparticle diffusion models, respectively;  $h$  ( $\text{mmol g}^{-1} \text{min}^{-1}$ ) is the initial sorption rate constant and  $C$  is the intercept.  $\alpha$  ( $\text{mmol g}^{-1} \text{min}^{-1}$ ) is the initial adsorption rate, and  $\beta$  ( $\text{g mmol}^{-1}$ ) is the constant of the degree of the surface coverage and activation energy for chemisorptions.

### 2.6.4. Thermodynamic parameters

The free energy change  $\Delta G_{\text{ads}}^\circ$  ( $\text{kJ mol}^{-1}$ ), enthalpy change  $\Delta H_{\text{ads}}^\circ$  ( $\text{kJ mol}^{-1}$ ), and entropy change  $\Delta S_{\text{ads}}^\circ$  ( $\text{J mol}^{-1}$ ) are thermodynamic parameters, which can be obtained using Eqs. (12) and (13):

$$\ln K_d = \frac{\Delta S_{\text{ads}}^\circ}{R} - \frac{\Delta H_{\text{ads}}^\circ}{RT} \quad (12)$$

$$\Delta G_{\text{ads}}^\circ = -RT \ln K_d \quad (13)$$

where  $R$  is a gas constant ( $8.314 \text{ J mol}^{-1} \text{ K}^{-1}$ ),  $T$  is the temperature (K), and  $K_d$  is the equilibrium constant ( $\text{L g}^{-1}$ ).  $K_d$  was calculated as follows.

$$K_d = \frac{C_o - C_e}{C_e} \frac{V}{W} \quad (14)$$

where  $C_o$  ( $\text{mmol L}^{-1}$ ) and  $C_e$  ( $\text{mmol L}^{-1}$ ) are the concentration of metal ions before adsorption and after adsorption, respectively;  $V$  is the volume of aqueous solution in (L), and  $W$  is the mass of adsorbent in gram. To calculate thermodynamic parameters,  $K_d$  should be dimensionless, when  $K$  is given in  $\text{L g}^{-1}$ , the value of  $K_d$  can be dimensionless by multiplying it by 1,000 (1 L = 1,000 mL) [39], the obtained value being denoted with  $K^o$ .

## 3. Result and discussion

### 3.1. Characterization of CuHCF/poly(MAA-co-IA) composite

FTIR verified the existence of CuHCF in the poly (MAA-co-IA) hydrogel. Fig. 1 shows FTIR spectra of the synthesized CuHCF, poly(MAA-co-IA) and CuHCF/poly(MAA-co-IA) composite. Fig. 1a shows the spectrum of CuHCF, which presented a band at  $2,083 \text{ cm}^{-1}$  caused by the stretching vibration of the ( $\text{C}\equiv\text{N}$ ) group, and the formed peaks at  $470\text{--}585 \text{ cm}^{-1}$  are attributable to the ( $\text{Fe}\text{--}\text{C}$ ) stretching [40]. The IR spectrum of poly(MAA-co-IA), Fig. 1b shows two strong bands at  $3,425$  and  $1,705 \text{ cm}^{-1}$  attributed to the O–H stretching vibration and C=O stretching vibration from acidic groups, respectively. Additionally, the peak at  $1,458 \text{ cm}^{-1}$  is due to the bending vibration of  $\text{CH}_2$  groups from IA. The spectrum for CuHCF/poly(MAA-co-IA) composite, Fig. 1c shows a sharp peak at  $2,083 \text{ cm}^{-1}$  because of the stretching vibration of ( $\text{C}\equiv\text{N}$ ) group similar to that found in Fig. 1a for CuHCF. The peaks at  $478\text{--}594 \text{ cm}^{-1}$  are attributable to the Cu–O stretching. The existence of these peaks suggested the interaction between COOH groups from MAA and IA and CuHCF, which indicates that CuHCF nanoparticles were encapsulated in poly(MAA-co-IA).

SEM and TEM analysis were measured to observe morphology, determine the particle size and distribution of CuHCF nanoparticles. The results showed that the particle size of CuHCF exhibited in nanoscale with an average diameter of  $35.8 \text{ nm}$  (Fig. 2). The SEM microscopy and elemental mapping were collected, and EDX spectra are shown in Figs. 3 and 4 for CuHCF/poly(MAA-co-IA) composite sample before and after  $\text{Cs}^+$  loading. The SEM image of the virgin adsorbent (Fig. 3a) shows an irregular and rough surface with porous surface morphology. The porosity of the adsorbent simplifies the transfer of  $\text{Cs}^+$  ions to the prepared CuHCF/poly(MAA-co-IA) composite surface. After  $\text{Cs}^+$  adsorption (Fig. 3b), the pores disappeared, and the surface became completely packed and smooth due to the adsorption of  $\text{Cs}^+$  ions. The EDX

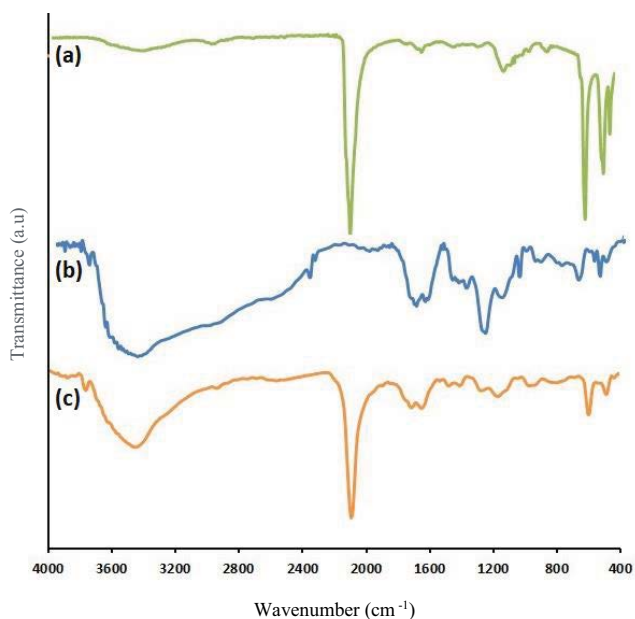


Fig. 1. FTIR spectra of the synthesized (a) CuHCF, (b) poly(MAA-co-IA) and (c) CuHCF/poly(MAA-co-IA) composite.

spectra in both samples show K, Fe, and Cu peaks representing the elemental constituents of CuHCF/poly(MAA-co-IA) composite before and after  $\text{Cs}^+$  loading (Fig. 3a and b). Additionally, EDX spectra (Fig. 3b) show Cs ion peak complemented with a decrease in the peak intensity of K. The EDX data (Fig. 3a and b) indicated that the atomic ratio of K/Fe of the virgin sample was 3.01, which is near to  $(\text{K}^+ \text{C})/\text{Fe} = 3.32$  in the adsorbent after  $\text{Cs}^+$  loading. The collected results showed that the adsorption process of  $\text{Cs}^+$  was done by ion exchange with  $\text{K}^+$ . Furthermore, the degree of exchange of  $\text{K}^+$  was calculated by dividing the difference in atomic % of K (13.46–9.47) over the atomic % of K before adsorption (13.46), and it was found to be 29.6%.

This percent reveals that 70.4% of the CuHCF/poly(MAA-co-IA) composite exchange centers are still free and available to exchange excess  $\text{Cs}^+$  from concentrated  $\text{Cs}^+$  solutions.

Fig. 4 shows the SEM-EDX elemental mapping of the virgin CuHCF/poly(MAA-co-IA) composite (Fig. 4a) and of Cs-loaded CuHCF/poly(MAA-co-IA) composite (Fig. 4b), the elemental mapping after adsorption of  $\text{Cs}^+$  showed the new and homogeneous distribution of  $\text{Cs}^+$  and less distribution of K.

The thermal properties of polymeric materials are significant for identifying and finally increasing their performance. Thermal performance of poly(MAA-co-IA) and CuHCF/poly(MAA-co-IA) composite was examined by TGA in the temperature range of 23°C–1,000°C under inert nitrogen atmosphere (Fig. 5). TGA curve for poly(MAA-co-IA) hydrogel, Fig. 5a, indicates an initial weight loss at around a range of 23°C–163°C, attributable to water adsorbed. The next weight loss in the range of 163°C–422°C attributable to the decarboxylation process (from MAA and IA), and the last one from 422°C to 489°C can be due to the cleavage of the main chain of the polymer. The TGA curve of the CuHCF/poly(MAA-co-IA) composite displayed a similar behaviour that poly(MAA-co-IA) while shifted to upper temperatures, Fig. 5b. This implies that the addition of CuHCF into hydrogel provided more thermal stability to the hydrogel. Additionally, DSC was tested for poly(MAA-co-IA) and CuHCF/poly(MAA-co-IA) composite. Two endothermic peaks in poly(MAA-co-IA) were detected at 114°C and 419°C, Fig. 5c, while the CuHCF/poly(MAA-co-IA) composite exhibited two endothermic peaks 247°C and 664°C, Fig. 5d.

Fig. 6 shows the XRD patterns of (a) poly(MAA-co-IA) hydrogel and (b) CuHCF/poly(MAA-co-IA) composite. As detected in Fig. 6a, there are no peaks in the XRD pattern of poly(MAA-co-IA) which indicated the amorphous nature of the polymer. The XRD pattern of CuHCF/poly(MAA-co-IA) presented different peaks at  $2\theta$  values of 18°, 25.6°, 35.9°, 39°, 45°, and 53° and 60° (Fig. 6b) [14,41,42]. The synthesized CuHCF/poly(MAA-co-IA) crystalline

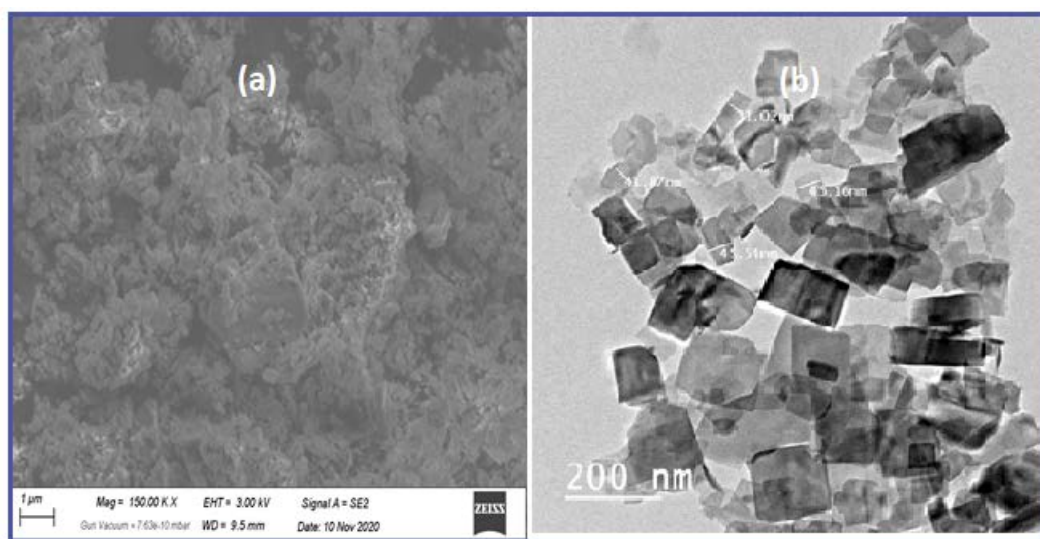


Fig. 2. (a) SEM and (d) TEM images CuHCF.

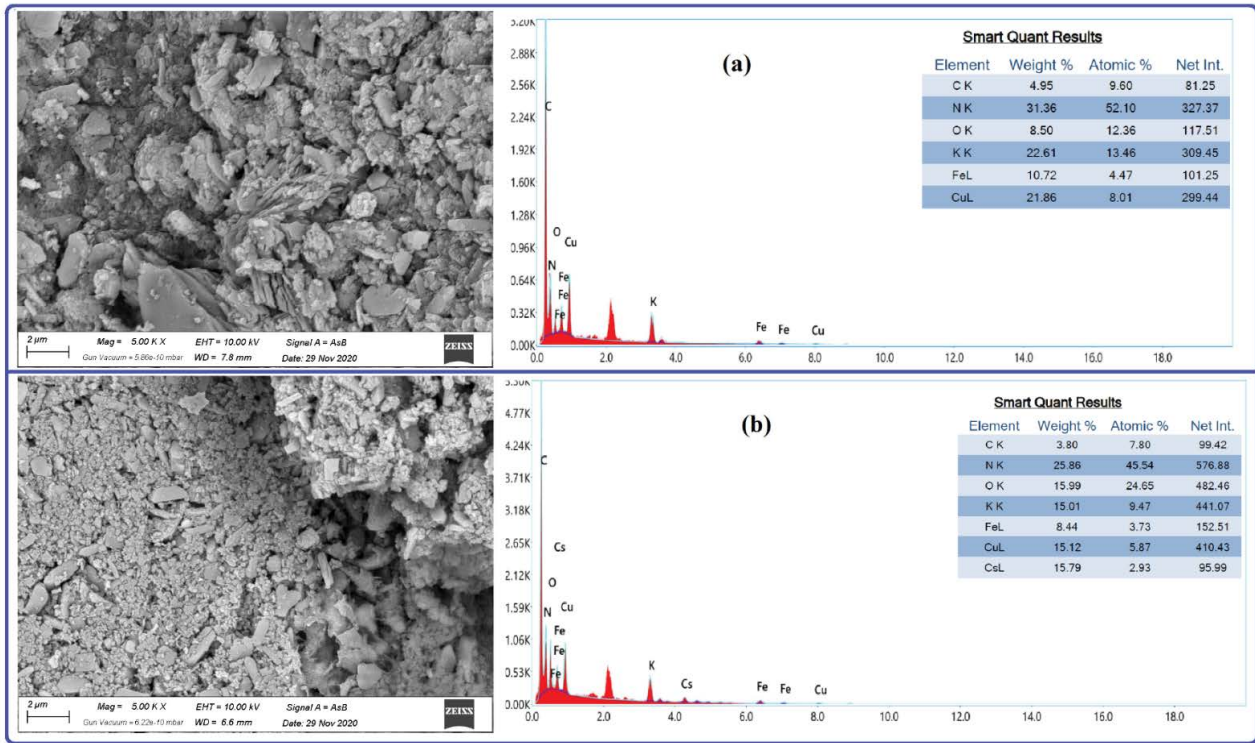


Fig. 3. SEM–EDX analysis of (a) CuHCF/poly(MAA-co-IA) before adsorption and (b) CuHCF/poly(MAA-co-IA) after cesium sorption.

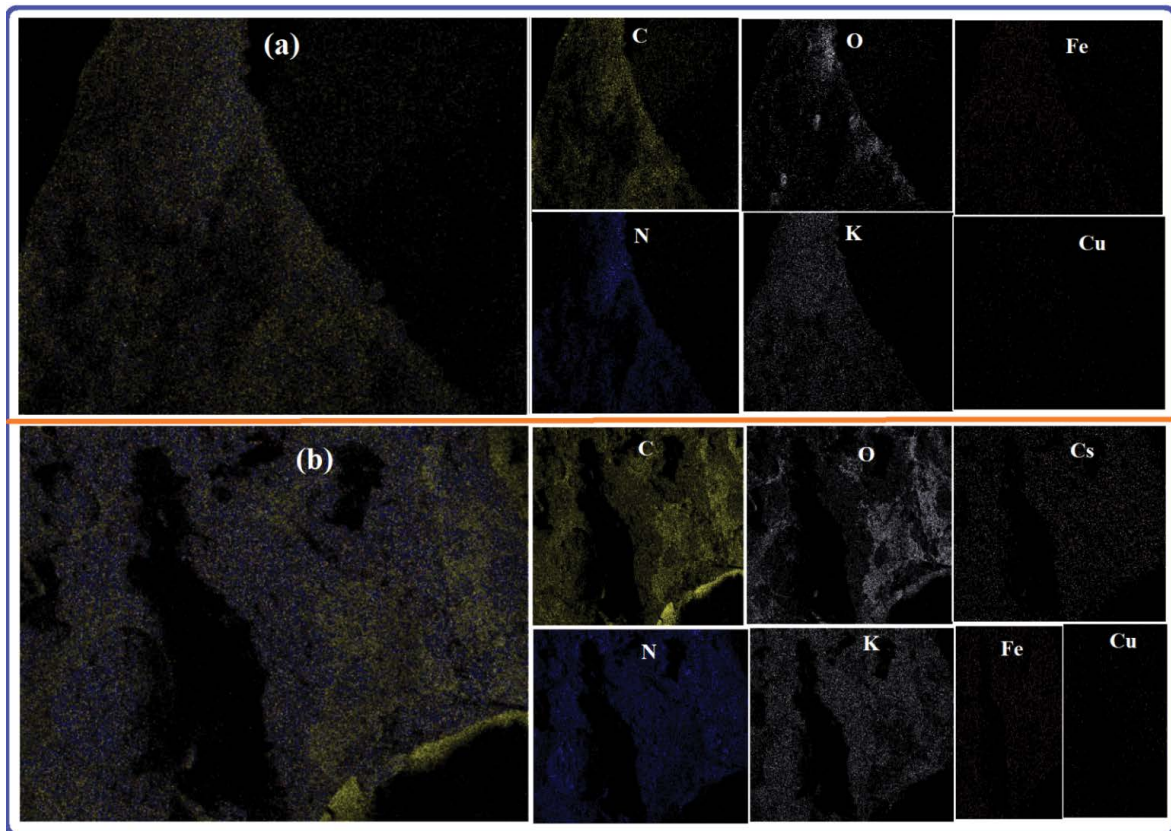


Fig. 4. Elemental mapping of CuHCF/poly(MAA-co-IA): (a) before cesium adsorption and (b) after cesium loading.

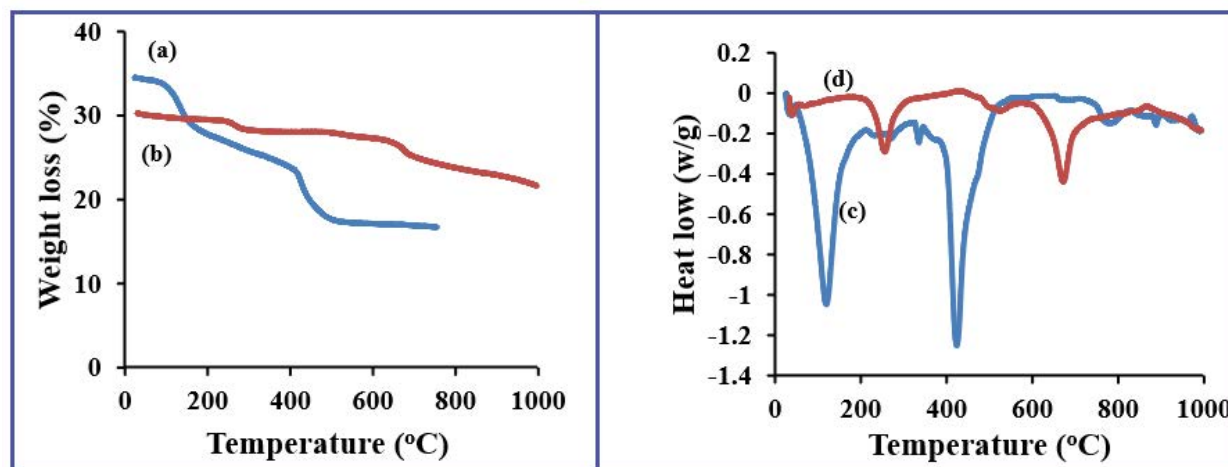


Fig. 5. Thermal analysis of (a,c) poly(MAA-co-IA) and (b,d) CuHCF/poly(MAA-co-IA).

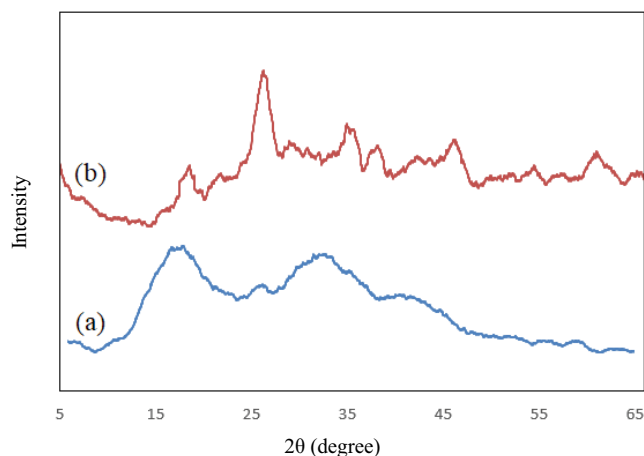


Fig. 6. XRD pattern of (a) poly(MAA-co-IA) and (b) CuHCF/poly(MAA-co-IA).

structure is compatible with that listed for CuHCF [21]. The indicated data shows that the nanoparticles of (CuHCF) are completely dispersed between the poly(MAA-co-IA) matrix.

### 3.2. Batch adsorption method

#### 3.2.1. Influence of pH

The stability and sorption properties of CuHCF/poly(MAA-co-IA) composite were examined at various pH conditions. The adsorption experiments were studied at 3 mmol g<sup>-1</sup> of Cs<sup>+</sup>, 25°C, and pH ranging from 2 to 12. As presented in Fig. 7, the adsorption capacity is continuously increased by increasing pH value from 2 to 9, and then, it decreased. While the adsorption process of Cs<sup>+</sup> in acid media decreased, the removal of Cs<sup>+</sup> using CuHCF/poly(MAA-co-IA) is still relatively high ( $q = 0.41 \text{ mmol g}^{-1} = 54.4 \text{ mg g}^{-1}$ ) in strong acid media at pH equal to 2. The maximum uptake of Cs<sup>+</sup> was observed in basic media at pH 9 ( $q = 0.88 \text{ mmol g}^{-1} = 116.9 \text{ mg g}^{-1}$ ); therefore, the following

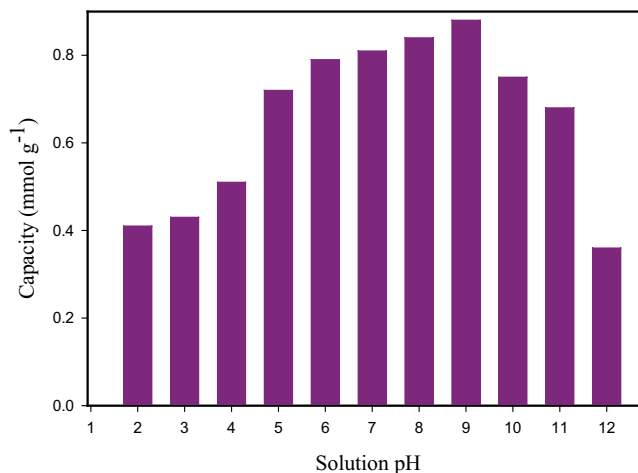


Fig. 7. Influence of pH on the adsorption of Cs<sup>+</sup> ions; 100 mL (3 mmol L<sup>-1</sup>), 0.1 g CuHCF/poly(MAA-co-IA), shaking time 4 h, and at room temperature.

tests in this article were carried out at pH equal to 9. When the pH increased from 9 to 12, the uptake process considerably decreased. In an acidic medium (pH = 2–4), the adsorption capacity has a low value which two reasons may cause. The first one is the sorption coemption between Cs<sup>+</sup> ions and hydrogen ions from COOH groups of the composite [14,43–45]. The additional cause is due to CuHCF/poly(MAA-co-IA) dissolution under acidic conditions [44]. In a strongly alkaline medium, the decrease in the adsorption process may be attributable to two reasons. The first one is the production of Cs(OH) ( $\text{Cs}^+ + \text{OH}^- \rightarrow \text{Cs(OH)}$ ) or negative ion form ( $\text{Cs(OH)} + \text{OH}^- \rightarrow \text{Cs(OH)}_2^-$ ). Cesium in both forms has a small attraction to the composite compared with positive form (Cs<sup>+</sup>) [44]. The second possible cause is fractional degradation of CuHCF from the composite surface in a basic medium, as shown in the earlier works [14,29]. It is important to mention that the uptake of Cs<sup>+</sup> from aqueous media using CuHCF/poly(MAA-co-IA) composite was comparatively greater than other adsorbents in

high acidic media (pH = 2–4). For this result, the synthesized CuHCF/poly(MAA-co-IA) composite showed a high affinity for Cs adsorption from an aqueous solution [44,45].

### 3.2.2. Effect of initial $\text{Cs}^+$ concentration and equilibrium isotherm models

Fig. 8 presents the effect of  $\text{Cs}^+$  concentrations on the adsorption capacity of CuHCF/poly(MAA-co-IA) composite. The effect of  $\text{Cs}^+$  concentrations was studied at the initial concentrations range 1–10  $\text{mmol L}^{-1}$  at room temperature and optimum pH. As indicated in Fig. 8, the amount of  $\text{Cs}^+$  adsorbed significantly increased at the low concentration range 1–6  $\text{mmol L}^{-1}$ . The adsorption capacity slowly increased at high  $\text{Cs}^+$  concentrations before reaching a plateau profile at the initial concentration of  $\text{Cs}^+$  equal to 8  $\text{mmol L}^{-1}$  (1,064  $\text{mg L}^{-1}$ ). The maximum uptake of  $\text{Cs}^+$  by the composite was calculated to be 1.48  $\text{mmol g}^{-1}$  (196.8  $\text{mg g}^{-1}$ ). Over 80% of adsorbed  $\text{Cs}^+$  was reached with an initial concentration lower than 5.0  $\text{mmol L}^{-1}$ , suggesting that the interaction of CuHCF/poly(MAA-co-IA) with  $\text{Cs}^+$  was significant even at relatively low  $\text{Cs}^+$  concentration in the solution (Fig. 8). These results indicate the higher efficiency of CuHCF/poly(MAA-co-IA) composite in  $\text{Cs}^+$  removal from aqueous media.

The Langmuir, Freundlich, Temkin and D–R isotherm model parameters are estimated using Eqs. (2)–(5) and summarized in Table 1. According to correlation coefficient ( $R^2$ ) values, we concluded that the Langmuir model ( $R^2 = 0.991$ ) was better to describe the experimental data than other isotherm models. These showed the chemisorption of  $\text{Cs}^+$

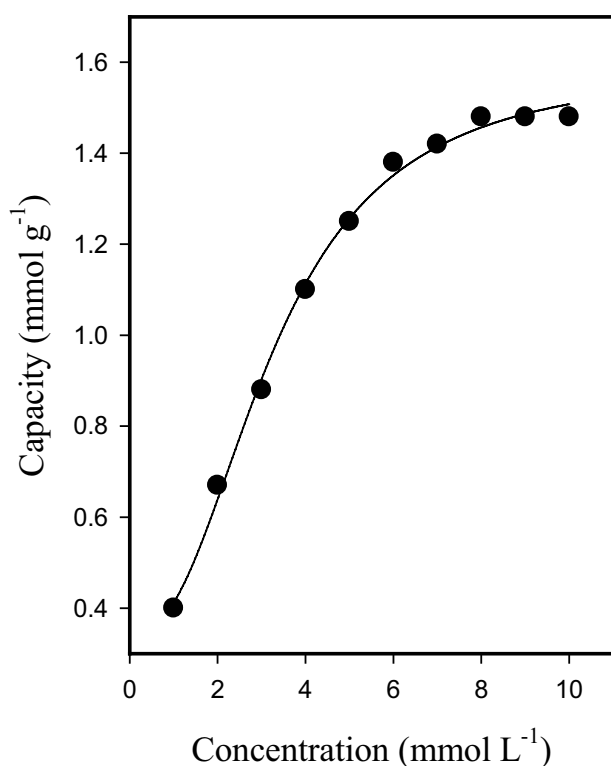


Fig. 8. Sorption isotherm of  $\text{Cs}^+$  using CuHCF/poly(MAA-co-IA) (concentration = 1.0–10  $\text{mmol L}^{-1}$ , 0.1 g adsorbent, solution pH = 9.0, shaking time 4 h at room temperature).

by CuHCF/poly(MAA-co-IA) can be monolayer adsorption on the homogeneous surface [46]. The calculated  $R_L$  values were found between 0.18 and 0.69 (Table 1), which implies that the adsorption of  $\text{Cs}^+$  is favourable at a higher initial concentration of  $\text{Cs}^+$  [47]. The magnitude of  $N$  value in Freundlich model ( $0 < N < 1$ ) signifies favorable adsorption condition [48]. From the D–R isotherm model, the values of mean free energy ( $E$ ) per molecule is 1581  $\text{kJ mol}^{-1}$  implies that the chemisorption process controls the uptake of  $\text{Cs}^+$ . The positive value of free energy ( $E$ ) showing that the adsorption of  $\text{Cs}^+$  by the composite is endothermic.

### 3.2.3. Comparison with other adsorbents

Commonly, the amount of  $\text{Cs}^+$  adsorbed by the composite ( $q_e$ ) is an important factor compared to other adsorbents. This work compares the present CuHCF/poly(MAA-co-IA) adsorbent with the latest results collected from various forms of CuHCF composites, as presented in Table 2. The results indicate that the amount of  $\text{Cs}^+$  adsorbed by CuHCF/poly(MAA-co-IA) is higher than most metal hexacyanoferrate composites [13–16,22–27]. However, the uptake of  $\text{Cs}^+$  by CuHCF/poly(MAA-co-IA) is lower than other adsorbents such as CuHCF-carbomer, amino-rGO/ZnHCF and (HEC + CMC) [21,28,29]. These collected data reveal that the CuHCF/poly(MAA-co-IA) composite is an effective adsorbent for removing  $\text{Cs}^+$  from an aqueous solution. It can be used to treat large volumes of radioactively contaminated water. Moreover, CuHCF/poly(MAA-co-IA) can be prepared with simple and inexpensive materials.

### 3.2.4. Effect of shaking time and equilibrium kinetic models

The kinetics of the adsorption process was examined by determining the adsorption capacity of  $\text{Cs}^+$  at various times. A series of experiments was conducted to determine the optimal shaking time for uptake of  $\text{Cs}^+$  onto CuHCF/

Table 1  
Parameters of Langmuir, Freundlich and Temkin isotherms and Elovich equation for adsorption of  $\text{Cs}^+$  on CuHCF/poly(MAA-co-IA)

Isotherm	Parameters	
	Parameter	Value
Langmuir isotherm	$Q_{\max}$ ( $\text{mmol g}^{-1}$ )	1.95
	$K$ ( $\text{L mmol}^{-1}$ )	0.434
	$R^2$	0.991
	$R_L$	0.18–0.69
Freundlich isotherm	$N$	0.506
	$K_f$ ( $\text{mmol g}^{-1}$ )	0.579
	$R^2$	0.958
Temkin isotherm	$K_T$ ( $\text{L g}^{-1}$ )	3.38
	$B$ ( $\text{J mol}^{-1}$ )	0.481
	$R^2$	0.985
D–R isotherm	$Q_{\max}$ ( $\text{mmol g}^{-1}$ )	1.36
	$K_{DR}$ ( $\text{mol}^2 \text{kJ}^{-2}$ )	$2 \times 10^{-7}$
	$E$ ( $\text{kJ mol}^{-1}$ )	1.581
	$R^2$	0.888

Table 2  
Cesium adsorption capacities from other composites listed in recently published articles

Support	Co-metal	Sorption capacity (mmol g <sup>-1</sup> )	Conditions	Ref.
Poly(MAA-co-IA)	Cu	1.48	pH 9.0, 25°C	This study
Carbomer	Cu	1.74	pH 9.0, 25°C	[29]
Poly-vinyl alcohol – sodium alginate (PVA-SA) nanofiber	Cu	0.86	pH 8, 25°C	[14]
HCF-Mbead	Cu	0.52	–, 25°C	[15]
Ammonium molybdophosphate-Polyethersulfone composite (AMP-PES)	Cu	0.42	–, 27°C	[16]
Hydroxyethyl cellulose-carboxymethyl cellulose (HEC + CMC)	Cu	2.32	pH 7.0, 25°C	[21]
CHCF/SBA-15	Cu	0.123	pH 7.0, 35°C	[22]
Bacterial cellulose membrane	Ni	1.32	pH 6, 25°C	[23]
MOF	Ni	1.15	pH 9.0, 25°C	[24]
Sericite	Ni	0.1	pH 5.0, 25°C	[25]
Chitin	Fe	0.32	pH 6.0, 20°C	[26]
Polyacrylonitrile	Fe	0.714	pH 7.0, 25°C	[27]
Amino-rGO/ZnHCF	Zn	1.998	pH 5.0, 25°C	[28]
Polyaniline	Co	1.36	pH 7, 60°C	[13]

poly(MAA-co-IA) composite in the shaking time range of 10 – 60 min. Contact time experiments were performed at optimum pH, Initial concentration of Cs<sup>+</sup> = 8 mmol L<sup>-1</sup>, and room temperature; the plot is shown in Fig. 9. As presented in Fig. 9, the amount of Cs<sup>+</sup> adsorbed by CuHCF/poly(MAA-co-IA) composite increased as contact time increased, then the equilibrium is attained as shown by a flat plateau. The rate of uptake was rapid, and the equilibration was achieved in 40 min. Half-load time ( $t_{1/2}$ ) was less than 10 min. This high initial adsorption rate towards Cs<sup>+</sup> indicates that the adsorption process occurs mainly on the composite surface and the regular distribution of CuHCF on poly(MAA-co-IA) surface, making the rapid Cs<sup>+</sup> uptake at the beginning of the experiment. The fast removal process decreased the time needed for the adsorption of Cs<sup>+</sup> from wastewater which reduced the costs for the operation. It is vital to compare the time needed to reach the equilibrium with previously prepared adsorbents. It was observed that the CuHCF/poly(MAA-co-IA) required less time to uptake Cs<sup>+</sup> than other adsorbents, such as metal-organic framework (MOF) [24], CuHCF-carbomer [29], (CoHCNF)@poly [13], CuHCF-PAN (polyacrylonitrile) [12] and amino-rGO/ZnHCF [28] which showed an experimental data of Cs<sup>+</sup> removal time 45, 60, 200, 280 and 360 min, respectively.

In the present work, four kinetic models were used to simulate the experimental data to clarify the main adsorption mechanism. These kinetic models included pseudo-first-order kinetic model [Eq. (8)], pseudo-second-order kinetic model [Eq. (9)], intraparticle diffusion model [Eq. (10)] and Elovich model [Eq. (11)]. The kinetic parameters and correlation factor ( $R^2$ ) were estimated and are listed in Table 3. According to values of  $R^2$ , it was found that both pseudo-second-order [35] and Elovich model [38] were up to 0.99, revealing that the adsorption of Cs<sup>+</sup> onto

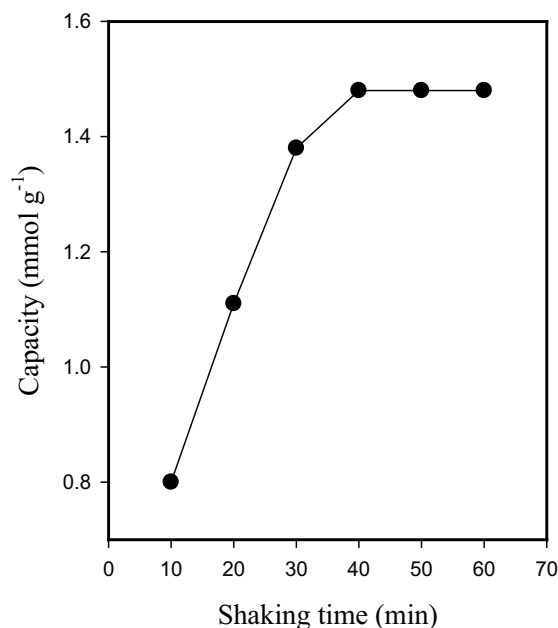


Fig. 9. Influence of contact time on the removal of Cs<sup>+</sup> using 0.1 g CuHCF/poly(MAA-co-IA) and Cs<sup>+</sup> concentration of 8.0 (mmol L<sup>-1</sup>) of Cs<sup>+</sup> at solution pH = 9.0 and at room temperature.

CuHCF/poly(MAA-co-IA) follows the chemisorption process [45]. This conclusion is reliable with the results listed for other polymer encapsulated potassium copper hexacyanoferrate composites [13,15,29]. The intraparticle diffusion plots for Cs<sup>+</sup> adsorption, as shown in Fig. 10, indicates multilinearity. The plot could be divided into three parts. This shows that intraparticle diffusion was not the only rate-controlling step. Therefore, adsorption kinetics

Table 3  
First-order, second-order intraparticle diffusion rate constants and D–R isotherm

Equations	Parameters	
Pseudo-first-order kinetic equation	$q$ (mmol g <sup>-1</sup> )	1.34
	$K_{\text{ads}}$ (min <sup>-1</sup> )	0.095
	$R^2$	0.957
Pseudo-second-order kinetics	$q$ (mmol g <sup>-1</sup> )	1.81
	$K_2$ (g mmol <sup>-1</sup> min <sup>-1</sup> )	0.51
	$h$ (mmol g <sup>-1</sup> min <sup>-1</sup> )	1.67
	$R^2$	0.991
Elovich equation	$\alpha$ (mmol g <sup>-1</sup> min <sup>-1/2</sup> )	0.24
	$\beta$ (g mmol <sup>-1</sup> )	1.98
	$R^2$	0.992
Intraparticle diffusion equation	$K_{\text{id}}$ (mmol g <sup>-1</sup> min <sup>-1/2</sup> )	0.149
	$C$ (mmol g <sup>-1</sup> )	0.441
	$R^2$	0.861

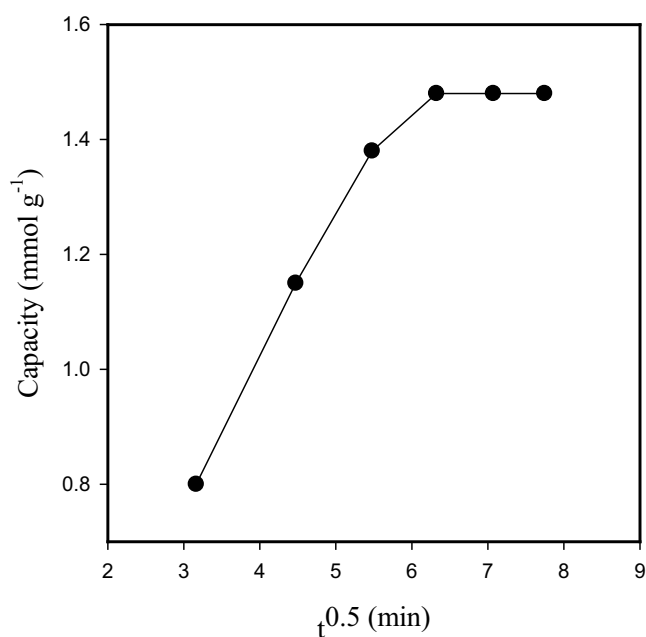


Fig. 10. Weber–Morris (intraparticle diffusion model) for the removal of Cs<sup>+</sup> using CuHCF/poly(MAA-co-IA).

can be limited simultaneously by intraparticle diffusion and film diffusion [29,37].

### 3.2.5. Influence of temperature and thermodynamic parameters

The influence of increasing temperature on the uptake of Cs<sup>+</sup> was studied with a temperature range of 25°C–55°C. The adsorption experiments were performed at pH 9, initial concentration of Cs<sup>+</sup> = 1 mmol L<sup>-1</sup>, and contact time = 40 min. The tabulated results reveal that ( $K^0$ ) of Cs<sup>+</sup> adsorption increased with increasing the temperature. The increase in  $K^0$  may be caused by the increase in kinetic

energy of Cs<sup>+</sup> and their mobility with increasing the temperature of the solution. To investigate the thermodynamic nature of the adsorption of Cs<sup>+</sup>, thermodynamic parameters including standard enthalpy ( $\Delta H_{\text{ads}}^{\circ}$ ), standard entropy ( $\Delta S_{\text{ads}}^{\circ}$ ), and standard Gibbs free energy ( $\Delta G_{\text{ads}}^{\circ}$ ) were calculated.  $\Delta H_{\text{ads}}^{\circ}$  and  $\Delta S_{\text{ads}}^{\circ}$  values were determined from the slope and intercept of the linear plot, Fig. 11, respectively. As indicated in Table 4, at all temperatures, the values of ( $\Delta G_{\text{ads}}^{\circ}$ ) were negative, which indicates the spontaneity and feasibility of Cs<sup>+</sup> adsorption. The negative value of Gibbs free energy ( $\Delta G_{\text{ads}}^{\circ}$ ) increased with increasing the temperature from 25°C to 55°C, which indicate that the spontaneity of the adsorption process is proportional to the temperatures. Furthermore, it reflects that the uptake of Cs<sup>+</sup> onto the composite surface is mainly chemisorption rather than physisorption [42]. The positive value of standard enthalpy ( $\Delta H_{\text{ads}}^{\circ}$ ) reflects the endothermic nature of Cs<sup>+</sup> uptake. The positive value of standard entropy ( $\Delta S_{\text{ads}}^{\circ}$ ) indicates the affinity of the prepared composite for Cs<sup>+</sup> and the increasing randomness at the (composite/Cs<sup>+</sup> solution) interface during the uptake process [24].

### 3.2.6. Selectivity and adsorption mechanism

A critical factor that affects the performance of an adsorbent for a metal under study is the selective adsorption of the metal ion in the existence of competitor ions. To confirm the selectivity of CuHCF/poly(MAA-co-IA) for Cs<sup>+</sup>, the distribution coefficient ( $K^0$ ) of Cs<sup>+</sup> was calculated in the existence of other monovalent cations (Cs<sup>+</sup>, Li<sup>+</sup>, Na<sup>+</sup>, K<sup>+</sup>) as well as the divalent cations, Ca<sup>2+</sup> and Mg<sup>2+</sup>. As indicated in Table 5, CuHCF/poly(MAA-co-IA) exhibited higher  $K^0$  value for Cs<sup>+</sup> (960.8 L g<sup>-1</sup>) compared with the  $K^0$  values for monovalent and divalent competing cations. This result indicates that CuHCF/poly(MAA-co-IA) has excellent selectivity for Cs<sup>+</sup>. The  $K^0$  values of monovalent cations are generally in the order Cs > Na > Li, which is the same order of hydrated ionic radius of the cations. This result is attributed to the smaller the hydrated ion that can easily reach the sorbent surface and, therefore, higher adsorption. The Cs-adsorption mechanism of CuHCF principally includes ion exchange

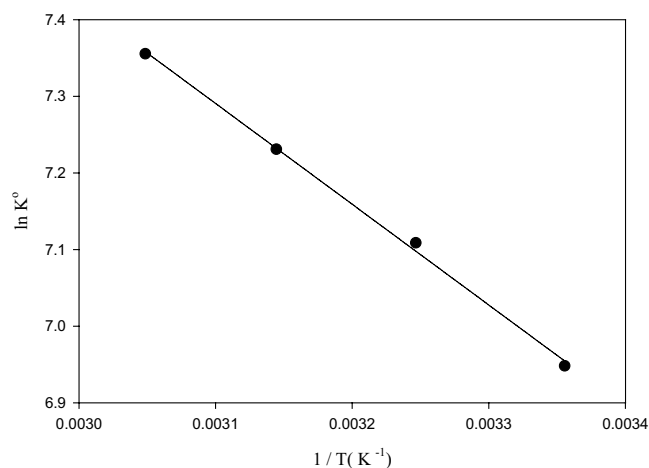


Fig. 11. The Arrhenius plot of  $\ln K^0$  against ( $T^{-1}$ ) for the removal of Cs<sup>+</sup> using CuHCF/poly(MAA-co-IA).

Table 4  
Thermodynamic parameters for the uptake of Cs<sup>+</sup> using CuHCF/poly(MAA-co-IA)

Temperature (K)	$K^{\circ}$ (L g <sup>-1</sup> )	$\Delta G_{\text{ads}}^{\circ}$ (kJ/mol)	$\Delta H_{\text{ads}}^{\circ}$ (kJ/mol)	$\Delta S_{\text{ads}}^{\circ}$ (J/mol)
298	1,040.816	-17.21		
308	1,222.222	-18.20		
318	1,380.952	-19.11	10.93	94.5
328	1,564.103	-20.05		

Table 5  
Selectivity of CuHCF/poly(MAA-co-IA) toward inactive Cs<sup>+</sup>

Ions	Concentration (mmol L <sup>-1</sup> )		$K^{\circ}$ (L g <sup>-1</sup> )	Hydrated ionic radius (Å)
	Before treatment	After treatment		
Cs <sup>+</sup>	1	0.51	960.8	2.26–2.28
Na <sup>+</sup>	1	0.81	234.6	2.76–3.6
K <sup>+</sup>	1	1.3	–	2.32–3.31
Li <sup>+</sup>	1	0.82	219.5	3.4–4.7
Ca <sup>2+</sup>	1	0.715	398.6	4.1
Mg <sup>2+</sup>	1	0.8	250	4.2

between Cs<sup>+</sup> in the diluted solution and potassium in the crystal structure of the composite, Fig. 12. As presented in Table 5, the total K<sup>+</sup> concentration in solution increased after the adsorption process by using CuHCF/poly(MAA-co-IA) in the presence of competing cations. This result indicates that ion exchange occurred between K<sup>+</sup> in CuHCF crystal and monovalent cation in the solution [49]. The adsorption of metal ion increase and exchange occur easily as the hydrated ionic radius of the metal ion close to that of K<sup>+</sup>. The increase of  $K^{\circ}$  value of divalent metal ions (Ca<sup>2+</sup> and Mg<sup>2+</sup>) may be due to complex formation between divalent metal ions and carboxylic groups of the polymer in CuHF/poly(MAA-co-IA). The uptake mechanism of Cs<sup>+</sup> by the composite is mainly an ion-exchange mechanism between Cs<sup>+</sup> in the solution and K<sup>+</sup> in CuHCF. The previously discussed data indicate that CuHCF/poly(MAA-co-IA) possesses higher selectivity toward Cs<sup>+</sup>.

### 3.2.7. Cs<sup>+</sup> desorption

Desorption of Cs<sup>+</sup> was studied using H<sub>2</sub>O, NaCl, NaOH, KOH, KCl, and HNO<sub>3</sub> (1 and 2 M) solutions. Fig. 13 indicates

that H<sub>2</sub>O could not recover more than 0.6% of adsorbed Cs<sup>+</sup>. 2 M KCl possesses a maximum recovery percent (98%). The desorbing agent with a concentration (2 M) has a higher desorption percentage than 1 M. Elution of Cs<sup>+</sup> with K<sup>+</sup> was more efficient than with Na<sup>+</sup> because of the closer hydrated ionic radius of K and Cs than that of Na and Cs; therefore, K could efficiently exchange with adsorbed Cs in the interior of CuHCF/poly(MAA-co-IA) composite.

## 4. Conclusion

In this work, we used a simple way to prepare novel composite material based on CuHCF nanoparticles incorporated in poly(MAA-co-IA) hydrogel matrix. The synthesized composite was characterized using different techniques such as FTIR, SEM, EDX, XRD, and TGA–DSC. The adsorption of Cs<sup>+</sup> using the prepared composite was studied by batch technique. The influences of essential factors such as pH, concentration, shaking time, solution temperature, and competing ions were examined. The results showed the maximum adsorption capacity of 1.48 mmol g<sup>-1</sup> at pH 9, 8 mmol L<sup>-1</sup> Cs<sup>+</sup>, and 25°C. The isotherm of the

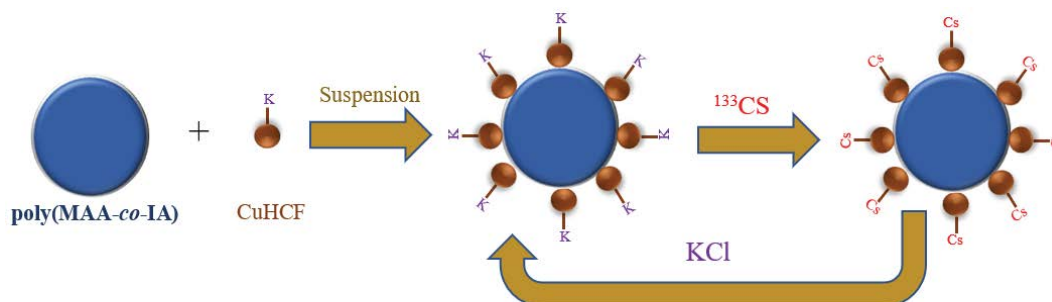


Fig. 12. Synthesis and adsorption–desorption cycles of CuHCF/poly(MAA-co-IA).

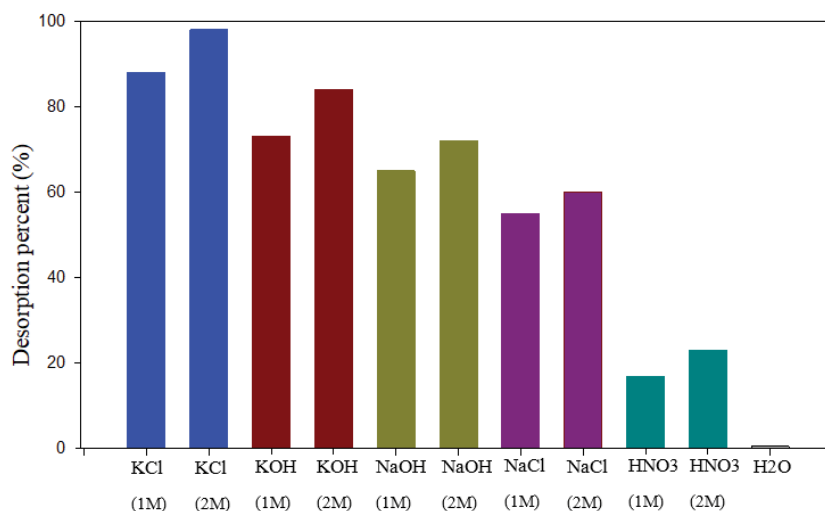


Fig. 13. Desorption of cesium by a different desorbing agents.

adsorption process was modeled by the Langmuir model. In the wide range of pH from 2 to 12, CuHCF/poly(MAA-co-IA) composite showed reasonable adsorption capacity even in a strongly acidic medium (pH 2) and a highly alkaline (pH 12) medium. The adsorption of Cs<sup>+</sup> was kinetically rapid, and the maximum amount of Cs<sup>+</sup> adsorbed attained in 40 min. According to the values of ( $R^2$ ) obtained for all tested kinetic models, the adsorption results can be modeled by both the pseudo-second-order model and the Elovich model. We were studying the adsorption process at different temperatures to calculate the thermodynamic parameters. The results indicated that the adsorption process was spontaneous in nature and endothermic. It was found that the CuHCF/poly(MAA-co-IA) possess remarkable selectivity towards Cs<sup>+</sup>. The desorption of Cs<sup>+</sup> was examined by different desorbing agents, and the result showed that elution of Cs<sup>+</sup> using 2 M KCl solution was favorite with maximum recovery percent (98%).

### Acknowledgement

The authors appreciatively acknowledge financial support from Taif University Researchers Supporting Project number (TURSP-2020/135), Taif University, Taif, Saudi Arabia.

### References

- [1] Y. Namiki, T. Namiki, Y. Ishii, S. Koido, Y. Nagase, A. Tsubota, N. Tada, Y. Kitamoto, Inorganic-organic magnetic nanocomposites for use in preventive medicine: a rapid and reliable elimination system for cesium, *Pharm. Res.*, 29 (2012) 1404–1418.
- [2] X. Liu, G.-R. Chen, D.-J. Lee, T. Kawamoto, H. Tanaka, M.-L. Chen, Y.-K. Luo, Adsorption removal of cesium from drinking waters: a mini review on use of biosorbents and other adsorbents, *Bioresour. Technol.*, 160 (2014) 142–149.
- [3] C. Vincent, Y. Barré, T. Vincent, J.-M. Taulemesse, M. Robitzer, E. Guibal, Chitin-Prussian blue sponges for Cs(I) recovery: from synthesis to application in the treatment of accidental dumping of metal-bearing solutions, *J. Hazard. Mater.*, 287 (2015) 171–179.
- [4] H.-M. Yang, K.-W. Lee, B.-K. Seo, J.-K. Moon, Copper ferrocyanide-functionalized magnetic nanoparticles for the selective removal of radioactive cesium, *J. Nanosci. Nanotechnol.*, 15 (2015) 1695–1699.
- [5] H. Yang, H. Li, J. Zhai, L. Sun, Y. Zhao, H. Yu, Magnetic prussian blue/graphene oxide nanocomposites caged in calcium alginate microbeads for elimination of cesium ions from water and soil, *Chem. Eng. J.*, 246 (2014) 10–19.
- [6] H. Yang, L. Sun, J. Zhai, H. Li, Y. Zhao, H. Yu, *In situ* controllable synthesis of magnetic Prussian blue/graphene oxide nanocomposites for removal of radioactive cesium in water, *J. Mater. Chem. A*, 2 (2014) 326–332.
- [7] C. Loos-Neskovic, S. Ayrault, V. Badillo, B. Jimenez, E. Garnier, M. Fedoroff, D.J. Jones, B. Merinov, Structure of copper-potassium hexacyanoferrate(II) and sorption mechanisms of cesium, *J. Solid State Chem.*, 177 (2004) 1817–1828.
- [8] T. Sangvanich, V. Sukwarotwat, R.J. Wiacek, R.M. Grudzien, G.E. Fryxell, R.S. Addleman, C. Timchalk, W. Yantasee, Selective capture of cesium and thallium from natural waters and simulated wastes with copper ferrocyanide functionalized mesoporous silica, *J. Hazard. Mater.*, 182 (2010) 225–231.
- [9] R. Chen, H. Tanaka, T. Kawamoto, M. Asai, C. Fukushima, M. Kurihara, M. Ishizaki, M. Watanabe, M. Arisaka, T. Nankawa, Thermodynamics and mechanism studies on electrochemical removal of cesium ions from aqueous solution using a nanoparticle film of copper hexacyanoferrate, *ACS Appl. Mater. Interfaces*, 5 (2013) 12984–12990.
- [10] Y. Zou, X. Wang, A. Khan, P. Wang, Y. Liu, A. Alsaedi, T. Hayat, X. Wang, Environmental remediation and application of nanoscale zero-valent iron and its composites for the removal of heavy metal ions: a review, *Environ. Sci. Technol.*, 50 (2016) 7290–7304.
- [11] J. Li, X. Wang, G. Zhao, C. Chen, Z. Chai, A. Alsaedi, T. Hayat, X. Wang, Metal-organic framework-based materials: superior adsorbents for the capture of toxic and radioactive metal ions, *Chem. Soc. Rev.*, 47 (2018) 2322–2356.
- [12] A. Nilchi, R. Saberi, M. Moradi, H. Azizpour, R. Zarghami, Adsorption of cesium on copper hexacyanoferrate-PAN composite ion exchanger from aqueous solution, *Chem. Eng. J.*, 172 (2011) 572–580.
- [13] T. Yousefi, M. Torab-Mostaedi, M.A. Moosavian, H.G. Mobtaker, Potential application of a nanocomposite: HCNFe@polymer for effective removal of Cs(I) from nuclear waste, *Prog. Nucl. Energy*, 85 (2015) 631–639.
- [14] Y. Kim, H.H. Eom, D. Kim, D. Harbottle, J.W. Lee, Adsorptive removal of cesium by electrospun nanofibers embedded with potassium copper hexacyanoferrate, *Sep. Purif. Technol.*, 255 (2021) 117745, doi: 10.1016/j.seppur.2020.117745.

- [15] Y.K. Kim, K. Bae, Y. Kim, D. Harbottle, J.W. Lee, Immobilization of potassium copper hexacyanoferrate in doubly crosslinked magnetic polymer bead for highly effective Cs<sup>+</sup> removal and facile recovery, *J. Ind. Eng. Chem.*, 68 (2018) 48–56.
- [16] J. Il Park, J.S. Kim, Y.B. Kim, H.J. Kwon, Y.J. Park, Evaluation of polyethersulfone-based composite for selective separation of cesium from acidic media, *Bull. Korean Chem. Soc.*, 37 (2016) 802–809.
- [17] S. Gaur, Determination of Cs-137 in environmental water by ion-exchange chromatography, *J. Chromatogr. A*, 733 (1996) 57–71.
- [18] D. Cuc, S. Bouguet-Bonnet, N. Morel-Desrosiers, J.-P. Morel, P. Mutzenhardt, D. Canet, Behavior of cesium and thallium cations inside a calixarene cavity as probed by nuclear spin relaxation. Evidence of cation- $\pi$  interactions in water, *J. Phys. Chem. B*, 113 (2009) 10800–10807.
- [19] E.H. Borai, R. Harjula, L. Malinen, A. Paajanen, Efficient removal of cesium from low-level radioactive liquid waste using natural and impregnated zeolite minerals, *J. Hazard. Mater.*, 172 (2009) 416–422.
- [20] H. Liu, A. Yonezawa, K. Kumagai, M. Sano, T. Miyake, Cs and Sr removal over highly effective adsorbents ETS-1 and ETS-2, *J. Mater. Chem. A*, 3 (2015) 1562–1568.
- [21] Y. Kim, Y.K. Kim, S. Kim, D. Harbottle, J.W. Lee, Nanostructured potassium copper hexacyanoferrate-cellulose hydrogel for selective and rapid cesium adsorption, *Chem. Eng. J.*, 313 (2017) 1042–1050.
- [22] S. Xiang, X. Zhang, Q. Tao, Y. Dai, Adsorption of cesium on mesoporous SBA-15 material containing embedded copper hexacyanoferrate, *J. Radioanal. Nucl. Chem.*, 320 (2019) 609–619.
- [23] S. Zhuang, J. Wang, Removal of cesium ions using nickel hexacyanoferrates-loaded bacterial cellulose membrane as an effective adsorbent, *J. Mol. Liq.*, 294 (2019) 111682, doi: 10.1016/j.molliq.2019.111682.
- [24] N. Genevois, N. Villandier, V. Chaleix, E. Poli, L. Jauberty, V. Gloaguen, Removal of cesium ion from contaminated water: improvement of Douglas fir bark biosorption by a combination of nickel hexacyanoferrate impregnation and TEMPO oxidation, *Ecol. Eng.*, 100 (2017) 186–193.
- [25] S. Naeimi, H. Faghihian, Performance of novel adsorbent prepared by magnetic metal-organic framework (MOF) modified by potassium nickel hexacyanoferrate for removal of Cs<sup>+</sup> from aqueous solution, *Sep. Purif. Technol.*, 175 (2017) 255–265.
- [26] T. Vincent, C. Vincent, Y. Barre, Y. Guari, G. Le Saout, E. Guibal, Immobilization of metal hexacyanoferrates in chitin beads for cesium sorption: synthesis and characterization, *J. Mater. Chem. A*, 2 (2014) 10007–10021.
- [27] Z. Jia, X. Cheng, Y. Guo, L. Tu, In-situ preparation of iron(III) hexacyanoferrate nano-layer on polyacrylonitrile membranes for cesium adsorption from aqueous solutions, *Chem. Eng. J.*, 325 (2017) 513–520.
- [28] J.-W. Choi, Y.-J. Park, H.-K. Lee, S.-J. Choi, Amine-functionalized graphene oxide/zinc hexacyanoferrate composites for cesium removal from aqueous solutions, *J. Radioanal. Nucl. Chem.*, 323 (2020) 785–793.
- [29] S.M. El-Bahy, D.A. Fadel, Z.M. El-Bahy, A.M. Metwally, Rapid and highly efficient cesium removal by newly synthesized carbomer encapsulated potassium copper hexacyanoferrate composite, *J. Environ. Chem. Eng.*, 6 (2018) 1875–1885.
- [30] I. Langmuir, The adsorption of gases on plane surfaces of glass, mica and platinum, *J. Am. Chem. Soc.*, 40 (1918) 1361–1403.
- [31] H. Freundlich, Adsorption in solution, *Phys. Chem. Soc.*, 40 (2009) 1361–1368.
- [32] M.J. Temkin, V. Pyzhev, Recent modifications to Langmuir isotherms, *Acta Physicochim. URSS*, 12 (1940) 217–222.
- [33] M.M. Dubinin, The Equation of the Characteristic Curve of Activated Charcoal, *Proceedings of the Academy of Sciences*, 1947, pp. 327–329.
- [34] S.M. El-Bahy, Z.M. El-Bahy, Immobilization of 2-amino pyridine onto poly(acrylonitrile-co-N,N-methylenebisacrylamide) nanoparticles for the removal of Hg(II), Cd(II) and Cr(III): batch and column techniques, *J. Environ. Chem. Eng.*, 5 (2017) 3560–3571.
- [35] S.K. Lagergren, About the theory of so-called adsorption of soluble substances, *Sven. Vetenskapsakad. Handlingar*, 24 (1898) 1–39.
- [36] Y.-S. Ho, Second-order kinetic model for the sorption of cadmium onto tree fern: a comparison of linear and non-linear methods, *Water Res.*, 40 (2006) 119–125.
- [37] W.J. Weber Jr., J.C. Morris, Equilibria and capacities for adsorption on carbon, *J. Sanit. Eng. Div.*, 90 (1964) 79–108.
- [38] S.H. Chien, W.R. Clayton, Application of Elovich equation to the kinetics of phosphate release and sorption in soils, *Soil Sci. Soc. Am. J.*, 44 (1980) 265–268.
- [39] S.K. Milonjić, A consideration of the correct calculation of thermodynamic parameters of adsorption, *J. Serbian Chem. Soc.*, 72 (2007) 1363–1367.
- [40] Z. Du, M. Jia, X. Wang, Cesium removal from solution using PAN-based potassium nickel hexacyanoferrate(II) composite spheres, *J. Radioanal. Nucl. Chem.*, 298 (2013) 167–177.
- [41] A. Takahashi, N. Minami, H. Tanaka, K. Sue, K. Minami, D. Parajuli, K.-M. Lee, S. Ohkoshi, M. Kurihara, T. Kawamoto, Efficient synthesis of size-controlled open-framework nanoparticles fabricated with a micro-mixer: route to the improvement of Cs adsorption performance, *Green Chem.*, 17 (2015) 4228–4233.
- [42] X. Wang, Y. Zhang, S. Jiang, X. Ji, Y. Liu, C.E. Banks, Cubic copper hexacyanoferrates nanoparticles: facile template-free deposition and electrocatalytic sensing towards hydrazine, *Int. J. Electrochem.*, 2011 (2011) 395724, doi: 10.4061/2011/395724.
- [43] Y. Kim, H.H. Eom, Y.K. Kim, D. Harbottle, J.W. Lee, Effective removal of cesium from wastewater via adsorptive filtration with potassium copper hexacyanoferrate-immobilized and polyethyleneimine-grafted graphene oxide, *Chemosphere*, 250 (2020) 126262, doi: 10.1016/j.chemosphere.2020.126262.
- [44] P.A. Haas, A review of information on ferrocyanide solids for removal of cesium from solutions, *Sep. Sci. Technol.*, 28 (1993) 2479–2506.
- [45] H. Yang, H. Li, J. Zhai, H. Yu, In situ growth of Prussian blue nanocrystal within Fe<sup>3+</sup> crosslinking PAA resin for radiocesium highly efficient and rapid separation from water, *Chem. Eng. J.*, 277 (2015) 40–47.
- [46] S.M. El-Bahy, New iminodiacetate chelating resin-functionalized Fe<sub>3</sub>O<sub>4</sub> nanoparticles: synthesis, characterization, and application for the removal of some noxious metal ions from wastewater, *J. Chem. Eng. Data*, 63 (2018) 2299–2313.
- [47] S.M. El-Bahy, Z.M. El-Bahy, Synthesis and characterization of polyamidoxime chelating resin for adsorption of Cu(II), Mn(II) and Ni(II) by batch and column study, *J. Environ. Chem. Eng.*, 4 (2016) 276–286.
- [48] S.M. El-Bahy, Z.M. El-Bahy, Synthesis and characterization of a new iminodiacetate chelating resin for removal of toxic heavy metal ions from aqueous solution by batch and fixed bed column methods, *Korean J. Chem. Eng.*, 33 (2016) 2492–2501.
- [49] H.-M. Yang, K.S. Hwang, C.W. Park, K.-W. Lee, Sodium-copper hexacyanoferrate-functionalized magnetic nanoclusters for the highly efficient magnetic removal of radioactive caesium from seawater, *Water Res.*, 125 (2017) 81–90.